Invited talk

NMR/NQR in the antiferromagnetic parent compounds of high-temperature superconductors

D. Brinkmann*

Physik-Institut, Universität Zürich, CH-8057 Zürich, Switzerland

Abstract

We review nuclear magnetic resonance (NMR) and nuclear quadrupole resonance (NQR) experiments performed in La_2CuO_4, $YBa_2Cu_3O_6$, and $Ca(Sr)CuO_2$ which are the antiferromagnetic parent compounds of some high-temperature superconductors. Both antiferromagnetic and paramagnetic phases are considered. The following topics are discussed: (1) Measurement and calculation of the sublattice magnetization (and hence the magnon excitation spectrum) in these compounds and its critical behavior; (2) low energy excitations in the antiferromagnetic phase of $Ca(Sr)CuO_2$; (3) various crossovers in $Ca(Sr)CuO_2$; (4) bilayer coupling in $YBa_2Cu_3O_6$. © 2001 Elsevier Science B.V. All rights reserved.

Keywords: NMR; NQR; High-temperature superconductors; Antiferromagnetic phase

1. Introduction

Many high-temperature superconductors can be derived, by doping or substitution, from antiferromagnetic (AF) parent compounds such as La_2CuO_4 (LACO for short), $YBa_2Cu_3O_6$ (YBCO6), and $Ca(Sr)CuO_2$ (CASCO). These structures are considered to be quasi-two-dimensional (2D) spin one-half ($S = 1/2$) Heisenberg antiferromagnets since the planar isotropic exchange coupling constant, J, is much larger than the inter-plane and the intra-plane $x - y$ constants, J' and J_{xy}, respectively. Although J' and J_{xy} are small, the J' coupling brings about 3D AF ordering at a finite temperature, the Néel temperature T_N, and the J_{xy} coupling forces the magnetic moments to lie parallel to the CuO_2 plane at temperatures $T < T_N$. Thus, the 3D ordered state is a peculiar AF state with extreme anisotropic exchange couplings.

Apart from the importance of their own, these AF structures are of interest for several other reasons. For instance: (i) There is the question about a possible interplay between magnetism and superconductivity. (ii) The magnetism of these compounds certainly reflects the strong electronic correlation that exists and that must be taken into account in any attempt to explain electron pairing in cuprates.

*Fax: +41-1-635-5704.

E-mail address: Detlef.Brinkmann@physik.unizh.ch (D. Brinkmann).

Methods especially suited to address these topics are nuclear magnetic resonance (NMR) and nuclear quadrupole resonance (NQR) since they probe directly the static and dynamic behavior at the atomic level. In this paper, we will review some studies in LACO, YBCO6, and CASCO which were performed in our laboratory and in collaboration with Prof. M. Matsumura of Kochi University (Japan). We will discuss the following examples: (1) General behavior of NMR and NQR frequencies; (2) the sublattice magnetization (and hence the magnon excitation spectrum) and its critical behavior; (3) calculation of the magnetization by the spin–wave model; (4) low energy excitations in the antiferromagnetic phase of CASCO; (5) various crossovers in CASCO; (6) bilayer coupling in YBCO6.

2. General behavior of NMR and NQR frequencies

We will start with some results about the general behavior of the Cu NMR and NQR frequencies in the AF ordered state. In this case, no external magnetic field is necessary and one performs NMR in zero external field. Since the orbital degeneracy at the planar Cu site is lifted by the crystalline field, the nuclear Larmor frequency, $\nu_L(T)$, is directly proportional to the sublattice magnetization, $M(T)$. Such Cu NMR measurements in the AF ordered states have been reported for LACO ($T_N = 312$ K)
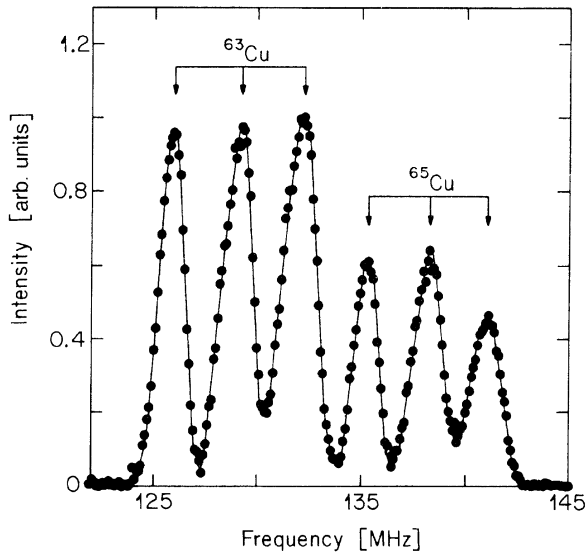
Fig. 1. ^{63}Cu and ^{65}Cu NMR spectra (in zero external field) of $Ca_{0.85}Sr_{0.15}CuO_2$ at 90 K. From Ref. [4].

Fig. 2. Temperature dependence of the ^{63}Cu Larmor frequency, ν_L, and quadrupole frequency (inset), ν_Q, in $Ca_{0.85}Sr_{0.15}CuO_2$. T_N indicates the Néel temperature. From Ref. [4].

[1], YBCO6 ($T_N \sim 420$ K) [2,3], and CASCO ($T_N = 540$ K) [4].

As an example, Fig. 1 shows the zero-field Cu spectrum in $Ca_{0.85}Sr_{0.15}CuO_2$ at 90 K [4]. [Since we will only deal with this specific doping, we will continue to use the general abbreviation CASCO.] The CASCO crystal structure consists of planar CuO_2 layers which, in contrast to the familiar Y–Ba–Cu–O compounds, contain no apical oxygen; the layers are separated from each other by alkaline earth atoms. The six peaks of the spectrum are attributed to the quadrupolar perturbed Zeeman transitions of the two Cu isotopes, ^{63}Cu and ^{65}Cu (nuclear spin = 3/2), in the internal hyperfine field, B_{hf}. Using standard procedures, we calculated, from the spectra, the Cu ν_L, which is proportional to B_{hf}, the quadrupolar frequency, ν_Q, which is a measure for the maximum component, V_{zz}, of the electric-field gradient tensor, present at the Cu sites, and the angle, θ, between B_{hf} and V_{zz}. The change with temperature of ^{63}Cu ν_L and ν_Q in CASCO is given in Fig. 2.

ν_Q allows us to draw some conclusions about the hole occupation in the Cu $3d_{x^2-y^2}$ orbital. In a semi-empirical approach, one assumes that ν_Q can be written as the sum of two terms: $\nu_Q = \nu_{VAL} + \nu_{LAT}$. The first term is the valence contribution arising from non-filled shells of the Cu ion under consideration, and the second term is the lattice contribution due to all charges outside this ion. ν_{LAT} can be written as $\nu_{LAT} = (1 - \gamma_\infty) \nu_{PCM}$. Here, γ_∞ is the Sternheimer antishielding factor and ν_{PCM} is calculated using the point charge model. It is natural to assume ν_{VAL} to be temperature independent. ν_{LAT} is negative and $|\nu_{LAT}|$ decreases with temperature because of the lattice expansion. In this way, the temperature dependence of ν_Q is explained.

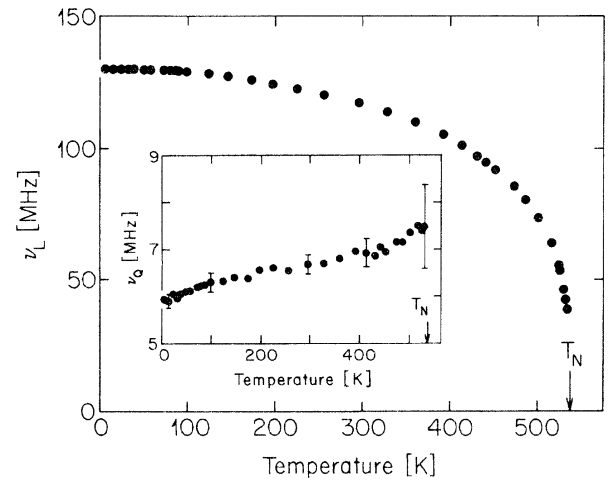Using the respective crystal structure data at 300 K, we

have calculated ν_{PCM} for the three AF insulators CASCO, YBCO6, and LACO and have fitted the experimental $^{63}\nu_Q$ values. The result is $(1 - \gamma_\infty) = 19.6(1.2)$, in agreement with the literature [5], and $\nu_{VAL} = 75.8(3.4)$ MHz. The fact that ν_{VAL} is approximately the same for all three structures implies that they have a similar Cu $3d_{x^2-y^2}$ hole occupation.

3. The sublattice magnetization

Next we will discuss ν_L of ^{63}Cu which is proportional to the hyperfine field, B_{hf}, at the Cu site. The accurate determination of B_{hf} allows one to determine the on-site static average magnetic moment within a constant factor. In 3D ordered systems, B_{hf} is expected to be strictly proportional to the macroscopic sublattice magnetization [6], M, whose temperature dependence, $M(T)$, reflects the nature of the spin interactions as well as their excitations. We will deal with two aspects, the low temperature dependence of $M(T)$ and its critical behavior near T_N.

In Fig. 3, we summarize the temperature dependence of the Cu quantity $1 - \nu_L(T)/\nu_L(0)$ for the three compounds LACO, YBCO6, and CASCO. The ordinate is proportional to the relative decrease of $M(T)$ and we note that it follows a power law: $[M(0) - M(T)]/M(0) = AT^n$, with the same exponent, $n \sim 2$. Only the prefactors A differ from compound to compound. This behavior of $M(T)$ suggests a common mechanism that causes the decrease of $M(T)$ with increasing temperature in all three compounds. Indeed, it is known that the decrease of $M(T)$ in AF compounds, at low temperatures, is caused by excitations of collective spin modes, such as spin waves. As we will show now, the behavior of $M(T)$ is well explained quantitatively within the framework of the linear spin–wave approximation for the quasi-2D $S = 1/2$ Heisenberg model.
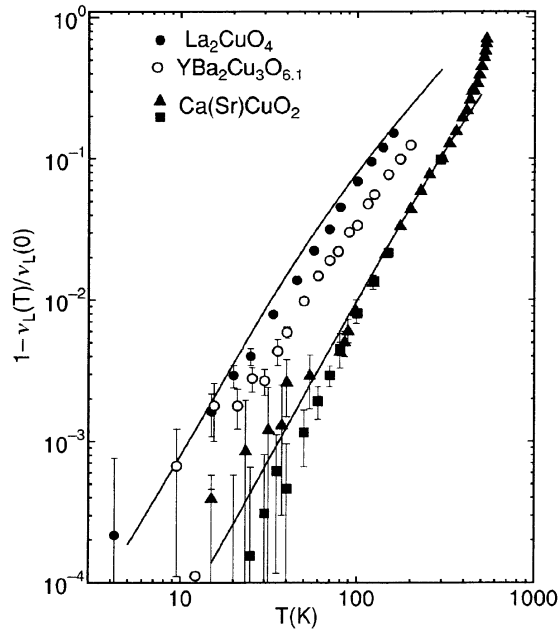
Fig. 3. The temperature dependence of the decrease of the Larmor frequency, $\nu_L(T)$, in La_2CuO_4 [1], $YBa_2Cu_3O_{6.1}$ [2], and $Ca(Sr)CuO_2$ (triangles from [4], squares from [7]). The solid lines for La_2CuO_4 and $Ca(Sr)CuO_2$ represent theoretical values calculated by means of the linear spin–wave model. From Ref. [7].

Fig. 4. Theoretical result (solid curve) and experimental data (filled symbols) for the relative decrease of the sublattice magnetization in $Ca(Sr)CuO_2$. IPA($\bigcirc$), OPA($\square$), IPO($\bigtriangledown$) and OPO($\diamondsuit$) refer to the contributions of the respective spin–wave modes. From Ref. [7].

For AF spin waves, of frequency $\omega(\mathbf{k})$ and wave vector $\mathbf{k}$, the reduction of $M(T)$ depends on whether the excitation spectrum is gapless or not. For $\omega(\mathbf{k}) = D\mathbf{k}$, i.e. a gapless spectrum, we have $[M(0) - M(T)]/M(0) \propto AT^\alpha$ ($\alpha \approx 2$); in case of $\omega(\mathbf{k}) = (E_g^2 + D\mathbf{k}^2)^{1/2}$, where E_g denotes the gap, the magnetization reduction is proportional to $\exp(-E_g/k_BT)T^{3/2}$. The experimental fact that $\alpha \approx 2$ in all three compounds, indicates that the gapless excitations dominate the decrease of the sublattice magnetization, at least from about 10 K to 100 K.

When numerically calculating $M(T)$ [1,2,7], four spin–wave modes have been considered: the in-plane acoustic (IPA), the out-of-plane acoustic (OPA), the out-of-plane optical (OPO), and the in-plane optical (IPO) modes, respectively. Because of the strong 2D nature of the exchange couplings, the spin–wave stiffness constant is very anisotropic. It is very large for an in-plane wavevector component $\mathbf{q}_\parallel = (k_x a, k_y a, 0)$, while it is very low for a component perpendicular to the plane, $\mathbf{q}_\perp = (0,0,k_z c)$. As a consequence, the spin–wave excitation energy has a deep dip in the neighborhood of $\mathbf{q}_\perp$. The decrease of $M(T)$ at low temperature arises from the low-lying spin–wave excitations. Excitations around $\mathbf{q}_\perp$ with long wavelength for the in-plane component are dominant in causing the magnetization decrease.

For the compound CASCO as an example, the results of the contribution of each mode and the total value of $[M(0) - M(T)]/M(0)$ are given in Fig. 4. The overall agreement with the experimental data is satisfactory. T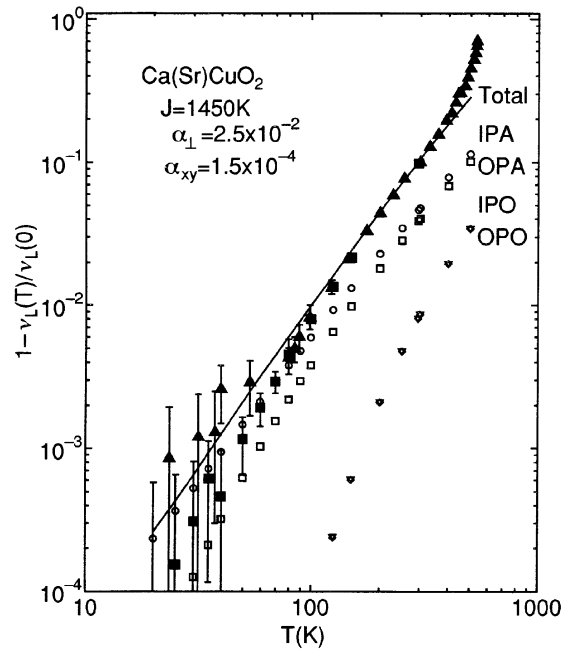he spin–wave excitation spectra in LACO and CASCO are very similar at long wavelengths, and the intra-layer couplings are nearly the same in both compounds. Hence, these two structures are ideal for addressing the question whether the different values of A are related, within the linear spin–wave model, to the different strengths of the *inter*-layer coupling. In Ref. [7], it is shown that, at very low temperatures, A is proportional to $(J'/J)^{-1/2}$.

The 'degree' of the 3D character in these quasi-2D compounds shows up in the way how rapidly $M(T)$ decreases with increasing temperature. For AF spin waves with linear dispersion, the density of states is proportional to ω and ω^2 in 2D and 3D systems, respectively. Consequently, systems with lower dimensionality have a larger spectral weight of low-energy thermal magnon excitations than 3D systems and hence M is more easily destroyed by thermal excitations in 2D than in 3D systems.

4. Critical behavior of sublattice magnetization

We now turn to the critical behavior of the normalized magnetization, $M(T)/M(0)$, which allows a quantitative statement about the *magnetic* dimensionality of CASCO [4]. Near T_N, the data should obey the 'critical equation' $M(T)/M(0) = (1 - T/T_N)^\beta$ where β is the critical exponent.

For an accurate determination of β and T_N we used the following fit-procedure [6]. The last 12 $M(T)/M(0)$ data points at temperatures just below T_N with T_{min} being the lowest temperature of this range, are fitted to the 'critical

equation' yielding the preliminary values $\beta^* = 0.273(2)$ and $T_N^* = 537.7(1)$ K. Then, the procedure is repeated with the last 11 data points (and a larger value of T_{min}) and so on until the last 6 data points, see left-hand side of Fig. 5. In this process, the seven values for both β^* and T_N^* increase asymptotically as shown in the right-hand side of Fig. 5. The final values are determined by means of the 'correction-to-scaling-method' [8] as represented by the two solid lines in the right-hand side of Fig. 5.

Our final result is: $\beta = 0.31(1)$ and $T_N = 539.0(5)$ K. The T_N value agrees with other values from the literature [9,10] but seems to be the most precise one at present. The value $\beta = 0.26(3)$ obtained for CASCO by a neutron scattering experiment [9] deviates appreciably from our final result but agrees with the preliminary value $\beta^* = 0.273(5)$ of our fit. We therefore suppose that the neutron data result is so low because a too large temperature region (290 to 550 K) was used for the fit.

When comparing our value for β with predictions made by various models for ordered magnetic systems [6], we note that our value is much larger than 0.125 as predicted for a 2D Ising model, but comes very close to the typical β for 3D systems: 0.325(2), 0.346(2) and 0.365(3) for the Ising, XY and Heisenberg model, respectively. That means that CASCO is more appropriately described by a 3D model whereas LACO and YBCO6 are typical examples of 2D structures. The fact that β in CASCO only comes close to rather than agrees with one of the theoretical values for a 3D system, can be explained by a cross-over of the structure to 3D behavior. These findings are in accord with our conclusions drawn from the low temperature behavior of the normalized magnetization.

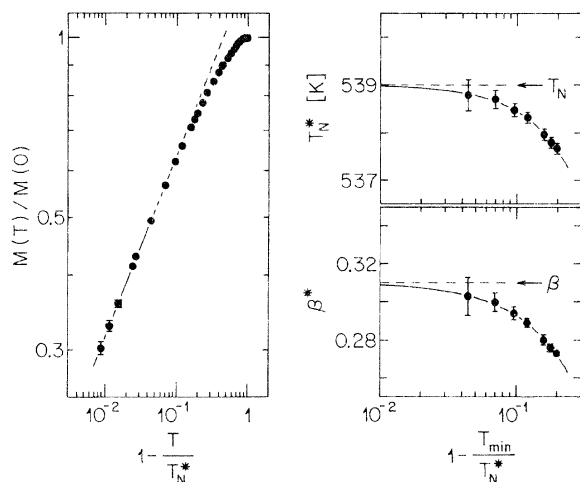We conclude this section with the remark that the degree

of the 2D AF character of these compounds can also be studied by *out-of-plane* nuclei such as Ba. We have performed such a Ba study for $YBa_2Cu_3O_{6.05}$ [11]. The internal magnetic field, $B(T)$, has been deduced from the modulation of the Ba NMR spin–echo intensity measured in an external magnetic field. A calculation of the dipolar field at the Ba site produced by $Cu(2)$ d electrons, yields a value that is about three times larger than the experimental result. The discrepancy could be explained by assuming that part of the magnetic moment is located at oxygen ions.

The temperature variation of $B(T)$ at the Ba site also follows, up to 402 K, a power law: $[B(0) - B(T)]/B(0) = AT^\alpha$ with $\alpha = 1.82(22)$ which agrees quite well with the results of the $Cu(2)$ in-plane determination of the sublattice magnetization [2,3,12]. Thus, $YBa_2Cu_3O_{6.05}$ behaves, in terms of its spin dynamics, as a quasi-2D antiferromagnet and this character can be studied at either out-of-plane Ba or in-plane $Cu(2)$ sites.

5. Low energy excitations in the antiferromagnetic state of CASCO

We will turn now to a *spin–lattice relaxation* study of the AF state of CASCO [13]. Relaxation measurements provide access to the dynamics at the atomic level of the sample. We will provide evidence for the presence of very light doping in the samples we have investigated. The doping has a profound effect on both the spin–lattice relaxation time, T_1, and the transverse relaxation time, T_2.

Chakravarty et al. [14] have treated in detail, within the framework of the spin–wave theory, nuclear spin–lattice relaxation in layered cuprate antiferromagnets. Among several possible relaxation mechanisms, the most effective ones are due to two and three magnon Raman scattering. The theory predicts a power law temperature dependence of $1/T_1$ and a strong dependence of $1/T_1$ on the anisotropy J'/J of the spin system.

Obviously, the experimental results of our work in CASCO (see Fig. 6) are not compatible with the power law prediction. The sizable maximum and the wide region of the temperature independent relaxation cannot be explained by any relaxation mechanism involving the population of a gas of Bose excitations like phonons or magnons: In fact, the number of these excitations and, therefore, the relaxation rate induced by them would increase monotonically with temperature.

We note that the two maxima are centered at the same temperature but differ in magnitude. This difference is proof for the presence of a different amount of holes in the two samples; the slight difference of the T_N values is another hint. We interpret the maximum in $1/T_1$ as evidence for the freezing of hole motion in the CuO_2 plane. These holes are strongly coupled to the AF spin system thus forming new quasi-particles called spin polarons. In the region occupied by a spin polaron the

Fig. 5. Procedure to determine the critical parameters β and T_N for $Ca_{0.85}Sr_{0.15}CuO_2$. Left: log–log plot of $M(T)/M(0) = (1 - T/T_N^*)^{\beta^*}$. The solid line is a fit to the last six data points below T_N. Right: Determination of the asymptotic values (dashed line) by the 'correction-to-scaling-method' which provides a fit (solid line) to the β^* and T_N^* data points, respectively. T_{min} denotes the lower limit of the temperature range used in the determination of the individual β^* and T_N^* data points. From Ref. [4].
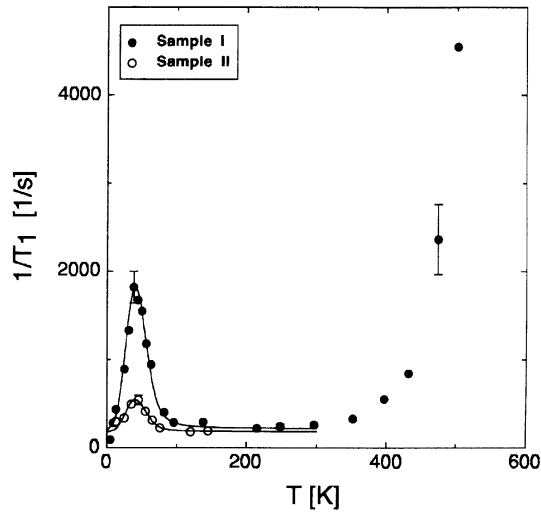
Fig. 6. ^{63}Cu spin–lattice relaxation rate, $1/T_1$, of two CASCO samples. The data is fitted for $T < 300$ K using the model described in the text. From Ref. [13].

order parameter, i.e. the internal field, is expected to be reduced. In this way when a hole gets into the proximity of a Cu nucleus, it induces a modulation of the hyperfine field which leads to fluctuations of the Cu nuclear Zeeman Hamiltonian and hence causes nuclear relaxation.

Since the details of the hole diffusion process are unknown, we refer to the phenomenological Bloembergen–Purcell–Pound (BPP) model of 'relaxation by diffusion' which has already been adapted to describe hole diffusion in another AF cuprate [15]. We therefore assume $1/T_1$ to be of the form

$$\frac{1}{T_1} = \gamma_n^2 \overline{H_{eff}^2} \frac{\tau}{1 + (2\pi\nu_L)^2\tau^2}, \qquad (1)$$

where γ_n is the nuclear gyromagnetic ratio, H_{eff} is the transverse component of some effective fluctuating local field, and τ is the correlation time of H_{eff} related to a thermally activated diffusion process. In our case, we identify τ with the inverse of the hole hopping rate. Thermally activated diffusion exhibits Arrhenius behavior, i.e. $\tau = \tau_0 \exp(E_a/kT)$ where E_a is an activation energy. The rate maximum occurs when $2\pi\nu_L\tau \approx 1$.

The BPP model is applicable under the condition that the weak-collision limit holds, that means a large number of fluctuations of H_{eff} are necessary to induce a nuclear transition. We assume that the hyperfine field, H_{hf}, is given by an on-site contribution plus a transferred contribution from the four neighboring Cu spins, so that an annihilation of a single spin leads only to a partial reduction of H_{hf}. Furthermore, in the low doping regime the hole is delocalized over a number of about 15 to 30 copper sites, as derived from the percolation threshold for the onset of metallic conductivity [16], so that the reduction of the AF field is shared by a large number of Cu sites.

To obtain the final $1/T_1$ expression, we modify Eq. (1) by: (i) adding a temperature independent 'background rate' term, R_B; (ii) expressing H_{eff} by fluctuating fields, H_x and H_y, oriented perpendicular to the AF field; (iii) introducing a Gaussian distribution $G(E)$ of activation energies, E, centered at $E = E_0$ and having a width ΔE. Hence, the final expression for the relaxation rate becomes

$$\frac{1}{T_1} = R_B + c\,\gamma_n^2\,(H_x^2 + H_y^2)\int_0^\infty \frac{G(E)\tau(E)}{1 + (2\pi\nu_L)^2\tau^2(E)}\,dE. \qquad (2)$$

The simultaneous fit of Eq. (2) to the experimental data of both samples [see Fig. 6] yields, among others, the parameters $\tau_0 = 2 \times 10^{-13}$ s, which is of the order of magnitude typical for electron motion, $E_0 = 27$ meV, and $\Delta E = 10$ meV. The value for E_0 is very close to those found for hole diffusion in Li doped CuO [15], where the hole concentration was larger than in our samples and where a doping dependence of the activation energy was determined. Further analysis of the data (see [13] for details) yields the concentrations $c_I \approx 4.9 \times 10^{-4}$ and $c_{II} \approx 1.1 \times 10^{-4}$.

The possible origin of the 'background rate', R_B, could be spin excitations induced by the presence of holes in the AF background. At temperatures higher than 350 K, $1/T_1$ diverges for $T \to T_N^-$ because of the slowing-down of magnetic fluctuations on approaching the phase transition. Unfortunately, we could not study the critical region because the ^{63}Cu NMR signal becomes too weak and broad at those temperatures and, above 504 K, it overlaps with the ^{65}Cu lines.

6. Electronic crossovers in the paramagnetic state of CASCO

The extension of our NMR study from the AF into the *paramagnetic* state of CASCO [17] revealed, among others, evidence for dimensionality and spin–degree crossovers of the magnetic structure. By *crossover* we refer to a *gradual* transition in contrast to a phase transition at a well defined temperature. The relaxation of Cu in CASCO arises predominantly from electron spin fluctuations, i.e. the relaxation mechanism is of magnetic rather than quadrupolar origin. We have measured the spin–lattice relaxation rates W_c (for $\mathbf{B}_0 \parallel c$ axis) and W_{ab} ($\mathbf{B}_0 \parallel ab$ plane); data for W_c are plotted in Fig. 7.

Three temperature regimes can be distinguished: (i) the high-temperature regime ($T > 600$ K) where data will be compared with the prediction for a spin-1/2 2D quantum Heisenberg antiferromagnet in the so-called renormalized classical (RC) regime; (ii) the regime between 600 K and T_N; (iii) the regime of critical behavior close to T_N.

The RC regime is governed by the critical slowing down of the spin fluctuations if the temperature approaches the

ordering temperature, $T_N^{2D} = 0$, of an ideal 2D quantum Heisenberg AF. In this regime, the low-energy spin dynamics are described in terms of the spin–wave stiffness constant, ρ_S, and the spin wave velocity, both being linear functions of the intraplanar coupling constant J [18]. The relaxation rate and the planar spin correlation length (normalized to the lattice constant a), ξ_{2D}, are then given by the relations [18,19]:

$$W_c = 0.3 \cdot \frac{(A_{ab} - 4B)^2}{J\hbar} \xi_{2D}(T) \cdot \frac{x^{3/2}}{(1+x)^2} \qquad (3)$$

$$\xi_{2D} = 0.5 \cdot \exp(1/x)[1 - (x/2) + O(x^2)], \qquad (4)$$

where $x = T/(1.13J)$. The spin hyperfine coupling constant, A_α^{spin}, can be written as $A_\alpha^{spin} = A_\alpha + 4B$, where A_α is the anisotropic on-site hyperfine coupling constant and B represents the transferred isotropic hyperfine coupling with one of the four nearest Cu neighbor spins in the plane [20]. Hence, the temperature dependence of W_c is dominated by the term $T^{1.5} \exp(1.13J/T)$. These equations seem to be valid up to $T = 2\rho_S = 1.13J/\pi \approx 550$ K [18] or even 1500 K according to Monte Carlo simulations [21].

In Fig. 7, we have plotted $W_c/T^{1.5}$–vs.–$1/T$, together with data for La$_2$CuO$_4$ [22]. Fitting Eq. (3) and Eq. (4) to our data in the temperature range 600 to 700 K, which excludes the critical region close to T_N, we obtain the parameters $J = 1450(150)$ K and $|A_{ab} - 4B| = 155(10)$ kOe μ_B^{-1}. The value of J is consistent with our estimate obtained from a magnetic shift analysis (not shown here) and it is in good agreement with the result, $J \approx 1535$ K, found by Raman scattering experiments [23]. Since J is an intrinsic property of the CuO$_2$ plane, its value is similar in related materials, for instance 1450(60) K in YBa$_2$Cu$_3$O$_{6.15}$ [24] and ≈ 1775 K in La$_2$CuO$_4$ [25].

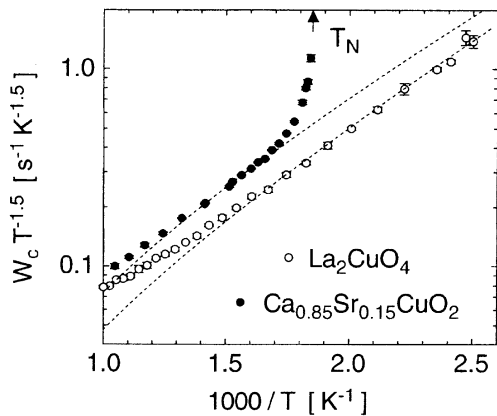The critical region in CASCO is somewhat uncertain, it is probably 10% of T_N. In this region we determined the
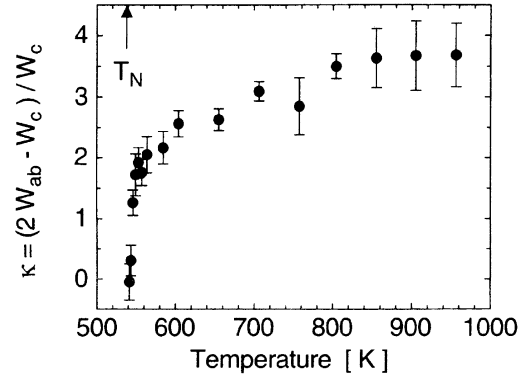

Fig. 8. The anisotropy of the ^{63}Cu spin–lattice relaxation rate, $\kappa = (2W_{ab} - W_c)/W_c$, as a function of temperature. From Ref. [17].

critical behavior of W_c which can be described by a power law: $W_c = C[(T - T_N)/T_N]^w$ with $w = -0.33(4)$. The value for w is identical with the value $-1/3$ calculated for the 3D Heisenberg model. This means that CASCO, which behaves as a 2D Heisenberg AF at high temperatures, undergoes, below approximately 600 K, a dimensionality crossover to a 3D Heisenberg AF.

Finally, very close to T_N, a second crossover takes place: a spin–degree crossover from the isotropic Heisenberg exchange interaction to a XY-like antiferromagnetism. This behavior is deduced from the strong temperature dependence of the anisotropy of the relaxation rate (between T_N and 600 K). We define the anisotropy by the ratio

$$\kappa = \frac{2W_{ab} - W_c}{W_c} = \frac{(A_c - 4B)^2}{(A_{ab} - 4B)^2} \cdot \frac{\chi_c''(\mathbf{Q}_{AF}, T)}{\chi_{ab}''(\mathbf{Q}_{AF}, T)} \qquad (5)$$

which is directly proportional to the ratio of the components of the dissipative electronic susceptibility at the AF wave vector. Our result is shown in Fig. 8. Since the coupling constants are temperature independent, the decrease of κ on approaching T_N from above shows that χ_c'' gets smaller with respect to χ_{ab}'' which implies that the electron spin fluctuations perpendicular to the plane become weaker than the in-plane fluctuations. This indicates the crossover to a XY-like antiferromagnetism. The reason for the crossover is the XY anisotropy which, in the AF ordered state, confines the spins to the plane [4].

7. Bilayer coupling in the paramagnetic phase of YBCO6

Our last section is devoted to a *bilayer* AF system in contrast to the *single-layer* systems of LACO and CASCO. There are considerable differences in the low-energy excitation spectra of bilayer systems in comparison with single-layer systems. In an intensive study of a single crystal of YBa$_2$Cu$_3$O$_{6.12}$ (YBCO6) [26], we have been

Fig. 7. $\log(W_cT^{-1.5})$ for Ca$_{0.85}$Sr$_{0.15}$CuO$_2$ (●) and La$_2$CuO$_4$ (○, data from Ref. [22]) as a function of inverse temperature. The dotted lines represent the respective fits to the RC prediction. The arrow indicates the Néel temperature of Ca$_{0.85}$Sr$_{0.15}$CuO$_2$. From Ref. [17].

dealing with, among others: (i) the determination of the planar correlation length in the renormalized classical regime; (ii) the rapid increase of the correlation length below 500 K and the determination of an effective AF in-plane coupling constant; (iii) the crossover from isotropic Cu(2) spin fluctuations at high temperature to XY-like fluctuations around T_N; (iv) the reduction of the Cu(2) magnetic moment due to quantum fluctuations and its relation to the number of layers; (v) the effect of the motion of remnant oxygen in the chains; and (vi) a possible explanation of the unusual increase of the [89]Y relaxation rate, measured previously, with rising temperature. Here, we will only address questions related to the bilayer correlation length.

In the previous Section, we discussed the Cu relaxation behavior in the RC regime of the paramagnetic state of CASCO and presented $W_c T^{-1.5}$ data for CASCO and LACO (see Fig. 7). In YBCO6, this quantity displays a behavior similarly to that of LACO for the temperature range 500 to 700 K. However, below 500 K, the YBCO6 data deviate from the curve for RC behavior; this fact is interpreted as the signature of the coupling of the layers into pairs. To show this, we plot, in Fig. 9, an 'experimental' correlation length, $\xi_{2D,exp}$, which we calculated by help of Eq. (3) using our $1/T_{1c}$ data, the value $|A_{ab} - 4B| = 117$ kOe μ_B^{-1} [obtained from a fit of Eqs. (3), (4) to the $W_c T^{-1.5}$ data in the 520–700 K temperature range], and $J = 1450$ K [24]. Obviously, $\xi_{2D,exp}$ displays a kink around 500 K and deviates from the curve for RC behavior thus

indicating the onset of intra-bilayer coupling. It turns out that the data below 500 K can be fitted by the expression $\xi_{2D,exp} = C(1 - x/2) \exp(1/x)$ with $x = T/1.13 J_{eff}$ which, in this form, is essentially the same as Eq. (4) that is valid for a *single* isolated layer. The best fit delivers $C = 1.14(80) \ 10^{-3}$ and $J_{eff} = 4120(300)$ K, where J_{eff} is approximately *three times* the value of J. This temperature dependence below 500 K implies a divergence of the bilayer correlation length at $T_N^{2D} = 0$ and is qualitatively different from the 3D critical increase of $1/T_1$ in CASCO at its finite Néel temperature, $T_N^{3D} = 539$ K (see [17]).

We now compare our results with two theoretical treatments. Recently, Yin et al. [27] have calculated the correlation length for a *bilayer* AF. The dotted line in Fig. 9 is their result for the specific value in YBCO6, $J_b/J = 0.08$, as obtained from neutron scattering [24]. This line obeys quite accurately the simple expression $\xi_{2D,bi} = C \exp(1.13 J_{eff}/T)$ with $C = 6.23(1.00) \ 10^{-2}$ and $J_{eff} = 3200(50)$ K. Compared with the two fits to our $\xi_{2D,exp}$ data below and above $T = 500$ K, the slope of the 'Yin curve' is too high at high temperatures and too low at temperatures close to T_N. In addition, the 'Yin curve' does not display the crossover behavior observed at $T = 500$ K and the absolute value of $\xi_{2D,exp}$ at 500 K is approximately one order of magnitude overestimated. Thus, the prediction for the bilayer structure in the RC regime is not as successful as that for the single-layer AF.

Next, we compare our data with Quantum Monte Carlo calculations [27,28] which have been performed to determine the correlation length for various values of the intra-bilayer coupling, J_b. The results of the two groups are shown in Fig. 9 by dashed [28] and dashed-dotted [27] lines. The curve for $J_b = 0$ confirms the analytical result of Eq. (4). The slopes of the other curves, for $J_b > 0$, seem to approach, at high temperature, the slope of the single-layer curve, and approach approximately the slope of our data at low temperatures, as soon as the calculated ξ_{2D} value exceeds ≈ 10 lattice constants. However, the predicted curve for $J_b/J = 0.08$ exhibits its 'kink' at much higher temperature than our experimental curve.

The discrepancy may be solved by either assuming that the Hamiltonian used in the calculation has to be improved by taking into account, for instance, a next-nearest neighbor coupling which markedly diminishes the correlation length or by postulating a much smaller bilayer coupling, for example $J_b/J \lesssim 0.01$. The apparent discrepancy with the neutron scattering result, $J_b/J = 0.08$, is not understood at present.
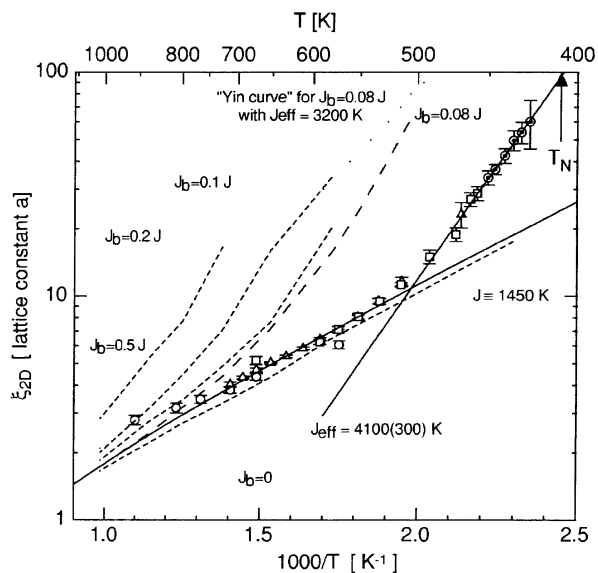

Fig. 9. The planar antiferromagnetic correlation length, ξ_{2D}, as a function of inverse temperature. The solid lines are fits to the experimental data above and below 500 K, respectively. The dotted line represents the prediction for a $S = 1/2$ bilayer quantum Heisenberg antiferromagnet in the renormalized classical regime [27] with $J_b/J = 0.08$. The dashed [28] and dashed-dotted [27] curves are the results of Quantum Monte Carlo calculations for bilayers with intra-bilayer coupling constants, J_b, ranging from $0.08J$ to $0.5J$. From Ref. [26].

8. Summary

Our discussion of NMR/NQR studies in the antiferromagnets La$_2$CuO$_4$ (LACO), YBa$_2$Cu$_3$O$_6$ (YBCO6), and Ca(Sr)CuO$_2$ (CASCO) has shown that these three com-

pounds share, in some cases, a common behavior while they exhibit quite different characteristics in other cases.

In all three compounds, the temperature dependence of the sublattice magnetization is quantitatively explained within the framework of the linear spin–wave approximation for the quasi-2D $S = 1/2$ Heisenberg model, resulting in a power law with the same exponent but differing prefactors which reflect the 'degree' of the 3D character. The numerical value of the critical exponent β reveals that CASCO is more appropriately described by a 3D model whereas LACO and YBCO6 are typical examples of 2D structures. The CASCO result can be explained by a dimensionality cross-over from the 2D Heisenberg AF to 3D behavior. Very close to T_N, a spin–degree crossover takes place from the isotropic Heisenberg to a XY-like interaction.

The renormalized classical regime has been studied by investigating the planar spin correlation length. In a certain temperature range, this quantity behaves the same way in all three compounds. The deviations in YBCO6 are the signature of the coupling of the layers into pairs. The temperature dependence of the correlation length implies a divergence which is qualitatively different from the 3D critical increase of the spin–lattice relaxation rate in CASCO at its finite Néel temperature. When comparing these data in YBCO6 with Quantum Monte Carlo calculations, agreement is only obtained if a very small bilayer coupling is postulated which disagrees with neutron scattering data.

Finally, an example demonstrates how manifold the results are one may obtain by investigating spin–lattice relaxation: the presence and motion of holes in the AF state of CASCO.

References

[1] M. Matsumura, M. Mali, J. Roos, D. Brinkmann, Phys. Rev. B 56 (1997) 8938.

[2] M. Matsumura, S. Nishiyama, Y. Iwamoto, H. Yamagata, J. Phys. Soc. Jpn. 62 (1993) 4081.

[3] C. Bucci, P. Caretta, D. Renzi, G. Guidi, S.G. Jang, E. Rastelli, A. Tassi, M. Varotto, Phys. Rev. B 48 (1993) 16769.

[4] A. Lombardi, M. Mali, J. Roos, D. Brinkmann, I. Mangelschots, Phys. Rev. B 54 (1996) 93.

[5] T. Shimizu et al., Bull. Magn. Resonance 12 (1990) 39.

[6] For instance, C. Hohenemser et al., Hyperfine Interact. 49 (1989) 267.

[7] M. Matsumura, F. Raffa, D. Brinkmann, Phys. Rev. B 60 (1999) 6285.

[8] See e.g.: H. Keller, I.M. Savić, Phys. Rev. B 28 (1983) 2638, and references therein.

[9] D. Vaknin et al., Phys. Rev. B 39 (1989) 9122.

[10] A. Keren et al., Phys. Rev. B 48 (1993) 12926.

[11] A. Lombardi, M. Mali, J. Roos, D. Brinkmann, Phys. Rev. B 53 (1996) 14268.

[12] Y. Iwamoto, M. Matsumura, H. Yamagata, K. Ishida, Y. Kitaoka, K. Asayama, H. Takagi, H. Iwabuchi, S.-I. Uchida, J. Phys. Soc. Jpn. 61 (1992) 441.

[13] F. Raffa, M. Mali, J. Roos, D. Brinkmann, M. Matsumura, K. Conder, Phys. Rev. B 58 (1998) 2724.

[14] S. Chakravarty, M.P. Gelfand, P. Kopietz, R. Orbach, M. Wollensak, Phys. Rev. B 43 (1991) 2796.

[15] P. Carretta, M. Corti, A. Rigamonti, Phys. Rev. B 48 (1993) 3433.

[16] M. Mehring, P. Gergen, C. Kessler, S. Krämer, in: E. Sigmund, K.A. Müller (Eds.), Phase Separation in Cuprate Superconductors, Springer, Berlin, 1994.

[17] R. Pozzi, M. Mali, M. Matsumura, F. Raffa, J. Roos, D. Brinkmann, Phys. Rev. B 56 (1997) 759.

[18] S. Chakravarty, R. Orbach, Phys. Rev. Lett. 64 (1990) 224.

[19] P. Hasenfratz, F. Niedermeyer, Phys. Lett. B 68 (1991) 231.

[20] F. Mila, T.M. Rice, Physica C 157 (1989) 561.

[21] M. Makivic et al., Phys. Rev. B 43 (1991) 3562.

[22] M. Matsumura, H. Yasuoka, Y. Ueda, H. Yamagata, T. Itoh, J. Phys. Soc. Jpn. 63 (1994) 4331.

[23] Y. Tokura, S. Koshihara, T. Arima, H. Takagi, S. Ishibashi, T. Udo, S. Uchida, Phys. Rev. B 41 (11) (1990) 657.

[24] S.M. Hayden, G. Aeppli, T.G. Perring, H.A. Mook, F. Dogan, Phys. Rev. B 54 (1996) R6905.

[25] S.M. Hayden, G. Aeppli, R. Osborn, A.D. Taylor, T.G. Perring, S. Cheong, Z. Fisk, Phys. Rev. Lett. 67 (1991) 3622.

[26] R. Pozzi, M. Mali, D. Brinkmann, A. Erb, Phys. Rev. B 60 (1999) 9650.

[27] L. Yin, M. Troyer, S. Chakravarty, Europhys. Lett. 42 (1998) 559.

[28] A.W. Sandvik, D.J. Scalapino, Phys. Rev. B 53 (1996) R526.